TRENDS IN SCIENCES 2025; 22(10): 10540
https://doi.org/10.48048/tis.2025.10540 RESEARCH ARTICLE

Phytochemical Profiling and Bactericidal Mechanism of *Crinum wattii* Extracts

Sirilak Kamonwannasit[1], Bung-on Prajanban[1], Orrasa Prasitnok[2], Piaw Phatai[3] and Agarat Kamcharoen[1,*]

[1]*Department of Agro-Industrial Product Development, Faculty of Agricultural Technology, Burapha University, Sakaeo, 27160, Thailand*
[2]*Department of Chemistry, Faculty of Science, Mahasarakham University, Maha Sarakham 44150, Thailand*
[3]*Department of Chemistry, Faculty of Science, Udon Thani Rajabhat University, Udon Thani 41000, Thailand*

([*]Corresponding author's e-mail: agratk@go.buu.ac.th)

Received: 2 May 2025, Revised: 26 May 2025, Accepted: 10 June 2025, Published: 30 July 2025

Abstract

Crinum wattii Baker, a perennial herb from the Amaryllidaceae family, was studied for its phytochemical content and antibacterial activity. Aqueous (AQE), ethanol (ETE), ethyl acetate (EAE), and chloroform (CFE) extracts from bulb samples were analyzed using colorimetric assays and high-performance liquid chromatography (HPLC). The ETE contained 47.93 mg/g of lycorine, suggesting its use as a quality control marker. AQE, EAE, and ETE showed high levels of tannins, flavonoids, and phenolics, respectively. Antibacterial activity was evaluated via disc diffusion method, revealing ETE as the most potent, especially against *Bacillus cereus* and *Bacillus subtilis*. Transmission electron microscopy (TEM) and scanning electron microscopy (SEM) revealed ETE-induced bacterial lysis and abnormal elongation, while Fourier Transform Infrared (FT-IR) spectroscopy indicated reductions in protein amides, polysaccharides, ester lipids, and nucleic acids, alongside an increase in phospholipids. These findings suggest that ETE disrupts bacterial protein, DNA, and cell wall synthesis in *Bacillus subtilis*, as evidenced by FT-IR analysis and ultrastructural changes. However, further molecular-level studies are required to identify the specific targets and mechanisms involved. In summary, *C. wattii* ETE, rich in lycorine and phenolics, exerts bactericidal effects through a lysis-based mechanism.

Keywords: Bactericidal activity, *Crinum wattii* extracts, Ethanolic extract, Lycorine alkaloid, Material characterization, Mechanism action, Phytochemical profiling

Introduction

Crinum wattii Baker, a perennial herbaceous plant of the Amaryllidaceae family, is found in Sa Kaeo province, Thailand. This plant family is known for its toxic alkaloid content, particularly concentrated in the bulbs, making them inedible. Despite their toxicity, Amaryllidaceae plants have been widely used in traditional medicine to treat infections, inflammation, and other ailments. Previous studies have demonstrated their pharmacological potential, including antioxidative, antimicrobial, anti-inflammatory, and anticancer activities [1-10]. However, little is known about the specific bioactive compounds responsible for these effects in *C. wattii*.

Our recent study evaluated the phytochemical composition, toxicity, and anti-inflammatory activities of *C. wattii* bulb extracts [11], but several critical gaps remained unaddressed. Specifically, no previous research had systematically compared the phytochemical content of *C. wattii* extracts obtained using different solvents (aqueous, ethanol, ethyl acetate, and chloroform), nor had the variations in phenolic, flavonoid, or tannin content across these extracts been evaluated. Furthermore, although alkaloids were reported in Amaryllidaceae plants, the presence and quantification of lycorine in *C. wattii* had not been investigated using high-performance liquid

chromatography (HPLC). In addition, no studies had assessed the antibacterial activity of *C. wattii* extracts against a panel of bacterial strains or explored the underlying bactericidal mechanisms.

Given these gaps, it is essential to consider the broader pharmacological importance of plant-derived alkaloids in relation to the therapeutic potential of *C. wattii*. Natural products, particularly plant-derived alkaloids and polyphenols, have been a consistent source of lead compounds in drug delivery [12-14]. Alkaloids, key secondary metabolites in plants, have demonstrated broad pharmacological applications, including in analgesia, cancer therapy, and infectious disease treatment [12-17]. Among these, lycorine, a major alkaloid in Amaryllidaceae species, exhibits antiviral, antitumor, antibacterial, and anti-inflammatory activities [3,10,18]. Various *Crinum* species serve as natural sources of lycorine [3,10,19] with studies indicating its strong antibacterial effects, particularly against both Gram-positive and Gram-negative bacteria. However, no research has quantified lycorine in *C. wattii*, and its antibacterial activity and mechanism of action remained completely unexplored prior to this study.

With increasing global concerns over antibiotic resistance, the search for novel, effective, and sustainable antimicrobial agents has become increasingly urgent. Natural products, particularly plant-derived compounds, are gaining renewed attention due to their diverse pharmacological properties and eco-friendly sourcing [12,13]. Recent studies have highlighted the potential of plant-based materials not only in direct antibacterial applications but also as agents or templates in nanomaterial synthesis for biomedical and environmental uses. For instance, green-synthesized ZnO nanoparticles [20], influenced by phytochemical-rich plant extracts, have shown promising results in degrading pollutants and inhibiting microbial growth. Likewise, biomass-derived organonanomaterials [21] have demonstrated utility in imaging and therapeutic applications, further underscoring the multifunctionality of plant-derived compounds. These advancements emphasize the importance of exploring underutilized medicinal plants such as *C. wattii*, which offer rich phytochemical reservoirs, including lycorine and phenolics that may serve both as antimicrobial agents and components of advanced bio-functional materials.

This study builds upon these concepts by exploring the phytochemical composition and antibacterial activity of *C. wattii* bulb extract. Lycorine was identified as a key compound, and its potential as a chemical marker for quality control is highlighted. Notably, the ethanolic extract (ETE) exhibited bactericidal effects against *Bacillus subtilis* by interfering with protein, DNA, and cell wall synthesis. This is the 1st report to (1) quantify lycorine in *C. wattii*, (2) evaluate antibacterial activity across extracts, and (3) reveal its bactericidal mechanism through ultrastructural and spectroscopic analysis. These findings support the potential of *C. wattii* as a natural antibacterial agent.

Materials and methods

Extract preparation

Fresh *Crinum wattii* bulbs were collected from Burapha University Sakaeo Campus, Sa Kaeo Province, and authenticated by Dr.Chakkrapong Rattamanee (Voucher specimen No. AgriTech-003). The bulbs were washed, chopped, oven-dried at 50 °C for 2 - 3 days, and ground into fine powder. For aqueous extract (AQE), 50 g of powder was boiled with 400 mL distilled water for 30 min. The mixture was filtered, centrifuged at 2,500 ×g for 10 min, and the supernatant was concentrated using a vacuum rotary evaporator.

Aqueous, ethanol, ethyl acetate, and chloroform were selected based on their differing polarities to extract a wide range of phytochemicals with varying solubility, allowing for comparative evaluation of phytochemical content and biological activity. The ethanol (ETE), ethyl acetate (EAE), and chloroform (CFE) extracts were prepared by separately extracting 50 g of powder with 95% ethanol, ethyl acetate, and chloroform using a Soxhlet apparatus. Each solvent extract was concentrated via vacuum evaporation, freeze-dried, and stored at 4 °C until use. Extract yields were calculated accordingly.

$$\text{Yield (\%)} = (\text{extract weight} / \text{bulb dried powder weight}) \times 100$$

Determination of alkaloids

Five grams of dried bulb powder were mixed with 200 mL of 10% acetic acid in ethanol and allowed to stand at room temperature for 4 h. The resulting mixture

was filtered, and the filtrate was concentrated using a water bath at 60 °C until the volume decreased to 25 mL. Ammonium hydroxide (NH_4OH) was then added dropwise to the concentrated extract until a precipitate formed. This precipitate was collected by filtration, dried, and weighed. The alkaloid content was subsequently determined and reported as a percentage.

Determination of tannins

The tannin content was determined using a modified method described by Palaniyappan *et al*. [22]. In brief, the extracts were dissolved in dimethyl sulfoxide (DMSO) at a concentration of 5 mg/mL. A 0.5 mL aliquot of each extract solution was combined with 3.75 mL of distilled water, 0.25 mL of Folin-Ciocalteu reagent, and 0.5 mL of 35% sodium bicarbonate. The mixture was incubated at room temperature for 30 min, after which the absorbance was recorded at 725 nm. All measurements were performed in triplicate. Tannin content was quantified using a tannic acid standard curve and expressed as micrograms of tannic acid equivalent (TAE) per gram of extract.

Determination of flavonoids

Total flavonoid content was assessed using the aluminum chloride ($AlCl_3$) colorimetric assay. In brief, extracts were dissolved in DMSO at a concentration of 5 mg/mL. A 50 µL aliquot of each extract solution was added to a 96-well plate, followed by 10 µL of 10% aluminum chloride, 150 µL of 95% ethanol, and 10 µL of 1 M sodium acetate. The mixture was incubated in the dark at room temperature for 40 min. Absorbance was measured at 415 nm using a microplate reader, with 95% ethanol as the blank. All assays were performed in triplicate. Flavonoid content was calculated using a quercetin standard curve and expressed as micrograms of quercetin equivalent (QE) per gram of extract.

Determination of phenolic compounds

A colorimetric method was used to determine the total phenolic content. Briefly, 2 mL of 2% Na_2CO_3 was added into 100 µL of a 2.5 µg/mL extract solution, and thoroughly mixed. After incubation at room temperature for 2 min, 100 µL of Folin-Ciocalteu chemical was added. The mixture was incubated in the dark at room temperature for 30 min, after which the absorbance was measured at 750 nm. All measurements were conducted in triplicate. Total phenolic content was determined using a gallic acid standard curve and expressed as milligrams of gallic acid equivalent (GAE) per gram of extract.

Determination of lycorine

The lycorine content was analyzed using high-performance liquid chromatography (HPLC) following a modified method by Ivanov *et al*. [23]. An Agilent 1260 Infinity II HPLC system was used for analysis. Chromatographic separation was achieved using a Poroshell 120EC-C18 column (150×4.6 mm^2, 4 µm) in a reversed-phase configuration. A gradient elution was employed with solvent A (1% ammonium acetate, pH 6.6) and solvent B (acetonitrile). Detection was performed at 287 nm using a diode array detector with a 16 nm bandwidth. The injection volume was 20 µL. Details of the gradient profile and flow rate are provided in **Table 1S**.

Determination of antimicrobial activity

The disc diffusion method was used to determine the antimicrobial activity of the bulb extracts [24]. Six bacterial strains were cultured in MHB at 37 °C, and 0.1 mL of each (10^8 CFU/mL) was spread on MHA. All extracts were reconstituted in 1% DMSO to a concentration of 300 mg/mL and applied consistently at 20 µL/disc for antibacterial testing. Extracts (6 mg/disc) were applied to sterile discs, with tetracycline and 1% DMSO as controls. Plates were incubated at 37 °C for 24 h to measure inhibition zones. *B. subtilis* and *B. cereus* were further tested for bactericidal activity. Extracts (0.625 - 10.0 mg/mL) were added to cultures and incubated. The minimum inhibitory concentration (MIC) and minimum bactericidal concentration (MBC) values were determined via turbidity measurement and colony observation on MHA. MIC was defined as the lowest concentration of the agent with no visible bacterial growth, whereas MBC was defined as the lowest concentration of agent required to kill the bacteria. Data were analyzed statistically using One-Way ANOVA with significance set at $p < 0.05$, and results were reported as mean ± standard deviation from triplicate experiments.

Characterization techniques

Bacillus subtilis cells were treated with ethanol extract (ETE), tetracycline (positive control), or left untreated, and incubated at 37 °C for 24 h. For Scanning Electron Microscopy (SEM), cells were fixed with glutaraldehyde, post-fixed with osmium tetroxide, dehydrated through serial ethanol concentrations, and analyzed using a Field Emission Scanning Electron Microscope (FE-SEM). For Transmission Electron Microscopy (TEM), cells were embedded in Spurr's resin, ultrathin sections were prepared, and counterstained with uranyl acetate and lead citrate, followed by analysis using a Tecnai G2 20 transmission electron microscope at 120 kV. Fourier Transform Infrared Spectroscopy (FT-IR) was performed by preparing cell suspensions, depositing them onto BaF_2 windows, and performing spectral analysis in the 4,000 - 900 cm^{-1} range. Spectra were collected on a Bruker Tensor 24 FT-IR spectrometer and proceed using Optical User Software (OPUS) 7.5 (Germany). FT-IR data were baseline-corrected, normalized, and processed using 2^{nd}-derivative filtering to enhance peak resolution. Principal component analysis (PCA) was then performed on selected spectral regions: 3,000 - 2,800 cm^{-1} (lipid CH stretching), 1,800 - 1,500 cm^{-1} (amide I and II), 1,500 - 1,200 cm^{-1} (nucleic acids and phosphates), and 1,200 - 900 cm^{-1} (polysaccharides and ester lipids). These regions were chosen based on their relevance to bacterial biomolecular structures. PCA loading plots were used to identify wavenumbers contributing to variance and to associate spectral shifts with biochemical changes such as membrane disruption or protein degradation.

Results and discussion

The dried powder of *C. wattii* bulbs contained 2.42% alkaloids. The yield and phytochemical composition of *C. wattii* bulb extracts are shown in **Table 1**. Among them, the aqueous extract (AQE) exhibited the highest yield (48.56%) and tannin content (61.78 ± 0.02 µg TAE/g), likely due to the high solubility of polar compounds like tannins in water. This suggests that water is effective for extracting tannin-rich fractions, making AQE particularly relevant for pharmacological applications. Water's low cost and environmentally further support its use in natural product research. The ethanolic extract (EAE) had the highest concentration of flavonoids (101.65 ± 4.68 µg QE/g), while the chloroform extract (CFE) and ethanol extract (ETE) had lower concentrations. In contrast, ETE contained the highest concentrations of total phenolic compounds (34.93 ± 1.32 mg GAE/g) and lycorine (47.93 mg/g) among all extracts. Lycorine content was quantified by HPLC, with chromatograms (**Figure 1**) confirming its presence in all extracts. The lycorine peak appeared at a retention time of 11.9 min in the standard (40 µg/mL), confirming lycorine as a key bioactive compound in these extracts. Therefore, lycorine can be used as a chemical marker for quality control of *C. wattii* bulb extracts.

The antibacterial activities of the extracts against *B. cereus* and *B. subtilis* are presented in **Table 2**. All extracts exhibited antibacterial activity, with the ETE showing the strongest inhibition zones. Additionally, the ETE inhibited the growth of all tested bacterial strains. Consequently, the ETE was selected for further investigation of its inhibitory and bactericidal effects against *B. cereus* and *B. subtilis*. The minimal inhibitory concentration (MIC) and minimal bactericidal concentration (MBC) of the ETE are shown in **Table 3**. The ETE exhibited the same MIC value (1.25 mg/mL) for both *B. cereus* and *B. subtilis*, but its bactericidal effect was stronger against *B. subtilis* (MBC 1.25 mg/mL) than against *B. cereus* (MBC 5 mg/mL). Therefore, the ETE was chosen for studying its bactericidal mechanism using SEM and TEM.

Table 1 Phytochemical composition of *C. wattii* tuber extracts.

Extracts	Yield (%)	Tannins (µg TAE/g)	Flavonoids (µg QE/g)	Phenolics (mg GAE/g)	Lycorine (mg/g)
AQE	48.56	61.78 ± 0.02	0.82 ± 0.04	24.54 ± 0.31	16.37
ETE	5.48	11.20 ± 0.12	5.89 ± 0.22	34.93 ± 1.32	47.93
EAE	0.65	1.69 ± 0.14	101.65 ± 4.68	27.19 ± 1.65	3.10
CFE	0.99	2.99 ± 0.23	64.78 ± 2.86	31.64 ± 2.43	4.13

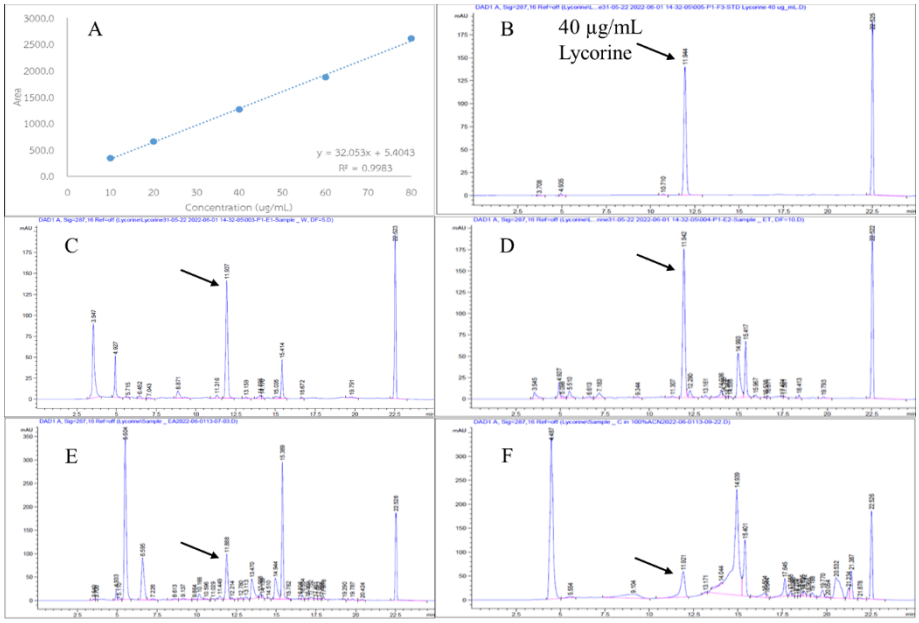

Figure 1 Standard curve of lycorine and its HPLC chromatogram from each extract. (A) Standard curve of lycorine. (B) HPLC chromatogram of standard lycorine. (C) HPLC chromatogram of lycorine from AQE. (D) HPLC chromatogram of lycorine from ETE. (E) HPLC chromatogram of lycorine from EAE. (F) HPLC chromatogram from CFE.

Table 2 Antibacterial activity of *C. wattii* tuber extracts.

Bacterial strains	Inhibition diameter (mm)				
	AQE (6 mg/disc)	ETE (6 mg/disc)	EAE (6 mg/disc)	CFE (6 mg/disc)	Tetracycline (30 µg/disc)
B. cereus	9.00 ± 0.64	18.98 ± 1.57	9.54 ± 0.94	12.29 ± 2.77	21.35 ± 0.89
B. subtilis	8.15 ± 3.15	16.94 ± 0.25	13.55 ± 0.95	19.96 ± 1.37	16.45 ± 2.22
E. coli	NA	10.03 ± 0.95	NA	8.83 ± 0.58	16.15 ± 2.64
P. aeruginosa	NA	10.62 ± 0.85	NA	NA	13.06 ± 1.45
S. aureus	NA	8.46 ± 1.14	NA	9.11 ± 2.07	19.28 ± 0.62
S. epidermidis	NA	9.82 ± 0.87	NA	8.90 ± 0.95	36.14 ± 1.89

Note: NA = no detection

The bactericidal effect of ETE was further examined using SEM and TEM. **Figure 2** shows SEM images of *B. subtilis* cells treated with 1.25 mg/mL ETE, which resulted in cell lysis (**Figure 2(B)**) compared with untreated cells (**Figure 2(A)**). The tetracycline-treated cells (**Figure 2(C)**) exhibited similar damage. In addition, the treated cells displayed filamentous shapes, indicating inhibition of cell division. TEM analysis (**Figure 3**) revealed damage to bacterial biomolecules and thinning of the cell walls in both ETE- and tetracycline-treated cells, suggesting cell wall degradation.

Table 3 Antibacterial activity of ETE against *B. cereus* and *B. subtilis*.

Bacterial trains	Antibacterial activity	
	MIC (mg/mL)	MBC (mg/mL)
B. cereus	1.25	5.00
B. subtilis	1.25	1.25

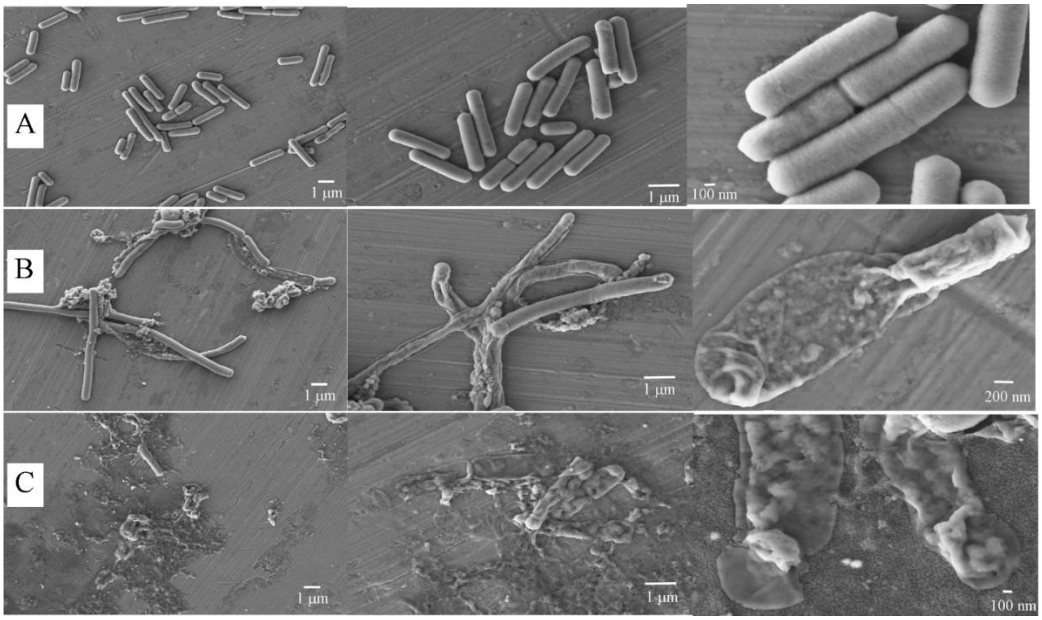

Figure 2 SEM images of treated *B. subtilis* cells. (A) Control or untreated cells. (B) ETE-treated cells. (C) Tetracycline-treated cells.

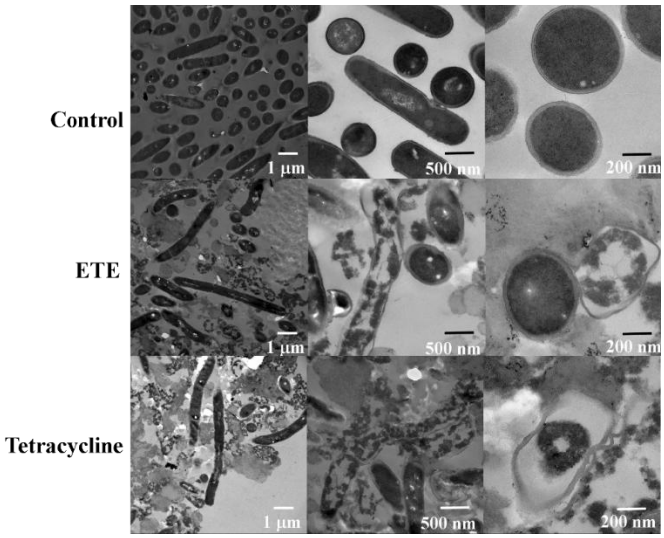

Figure 3 TEM images of treated *B. subtilis* cells. (A) Control or untreated cells. (B) ETE-treated cells. (C) Tetracycline-treated cells.

The FT-IR spectra from bacterial cell samples were appeared the peaks in the range of 3,000 - 2,800 and 1,800 - 900 cm^{-1} which are the spectrum range of phospholipid (3,000 - 2,800 cm^{-1}), protein (1,700 - 1,500 cm^{-1}) and polysaccharide (1,200 - 900 cm^{-1}) (**Figure 4**). To compare the difference of biomolecules in bacterial cells, the PCA score plot was used to analyze the spectra in range of 3,000 - 2,800 and 1,800 - 900 cm^{-1} from each sample. The results showed that the difference between 3 clusters of data was 89% and the T cluster was different from P and C clusters (**Figure 5**). The T cluster was located separately in the negative score of PC1 while the P and C clusters were in the positive score of PC1. Based on the comparison between the PCA score plot and loading plot (**Figure 6**), the peak corresponding to $-CH_2$ and $-CH_3$ groups of phospholipid (2,921 and 2,852 cm^{-1}) contributed to 56% of the variance explained by loading PC1. The C cluster was separated from those P and T clusters at the peaks of protein amide I (1,660 cm^{-1}), protein amide II (1,550 cm^{-1}), and protein amide III (1,235 cm^{-1}). While the P cluster was separated from those C and T clusters at the peaks of polysaccharide (1,153 and 1,027 cm^{-1}).

Moreover, nucleic acid (1,080 cm^{-1}) had variable value of 36% from loading PC2 (**Figure 5**) which correlated with the average spectra from 2nd derivative results in **Figure 7**. These spectral shifts suggest that ETE induces structural alterations in proteins, disrupts lipid membranes, and affects nucleic acid integrity, supporting the antimicrobial effects observed.

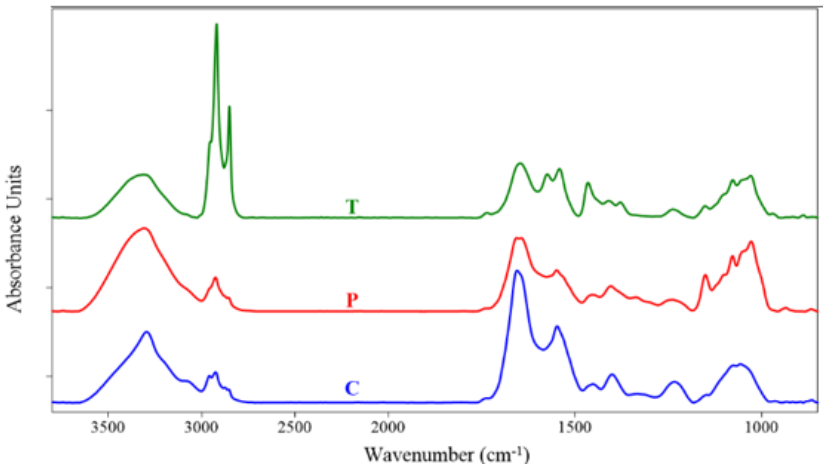

Figure 4 Spectrum of infrared adsorption from treated *B. subtilis* cells. When sample C is control or untreated cells, sample P is positive control or tetracycline treated cells, and sample T is testing sample or ETE treated cells.

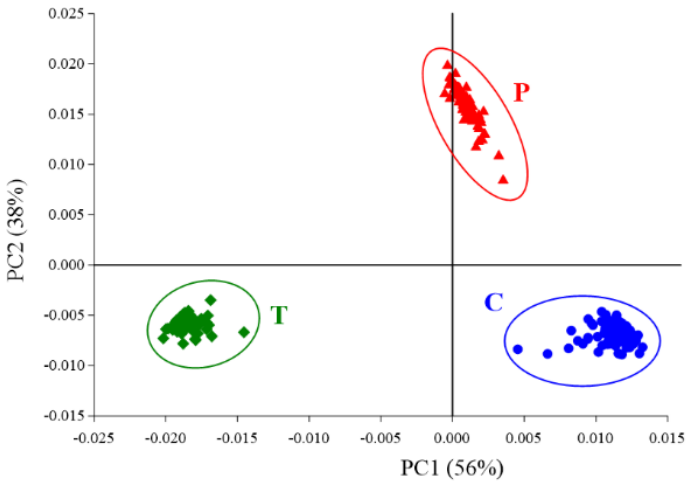

Figure 5 PCA score plot of spectrum from treated *B. subtilis* cells. When sample C is control or untreated cells, sample P is positive control or tetracycline treated cells, and sample T is testing sample or ETE treated cells.

The peak area of functional groups in bacterial cells was quantified (**Figure 8** and **Table 4**). The phospholipid peak (3,000 - 2,800 cm^{-1}) was significantly higher in the ETE-treated cells compared to both the control and tetracycline-treated cells. In contrast, the control cells exhibited higher levels of ester lipids, protein amide I (1,700 - 1,600 cm^{-1}), protein amide II (1,600 - 1,500 cm^{-1}), and protein amide III (1,300 - 1,200 cm^{-1}), whereas the tetracycline-treated cells had higher polysaccharide and nucleic acid peak areas.

The various extracts of *C. wattii* bulbs exhibited different phytochemical contents. Among these, the ethanolic tuber extract (ETE) contained higher concentrations of total phenolic compounds and lycorine, which aligns with our previous findings of stronger antioxidant activity in ETE compared to other extracts. This enhanced antioxidant activity is likely due to the abundance of phenolics and lycorine, both known for their bioactivity. The ethanolic extract (ETE) showed the highest levels of total phenolic compounds and lycorine, a major pyrrolophenanthridine alkaloid

from the Amaryllidaceae family known for its antibacterial activity. Phenolic compounds disrupt bacterial cell walls and membranes, increasing permeability and causing damage, while lycorine interferes with protein synthesis and induces oxidative stress. Together, these constituents likely act synergistically, enhancing ETE's potent antimicrobial effects, especially against *Bacillus* species that are sensitive to cell wall disruption and metabolic interference. Although lycorine is probably the main contributor, the interaction with phenolics and other bioactive compounds may broaden and strengthen the antibacterial activity. Further studies using compound isolation and bioassay-guided fractionation are needed to clarify these synergistic effects. Previous research has highlighted lycorine's antioxidant effects, which may contribute to its medicinal properties [25]. The HPLC analysis in this study confirmed that lycorine was one of the key alkaloid bioactive compounds in *C. wattii* bulbs, and it can potentially serve as a chemical marker for quality control of *C. wattii* extracts.

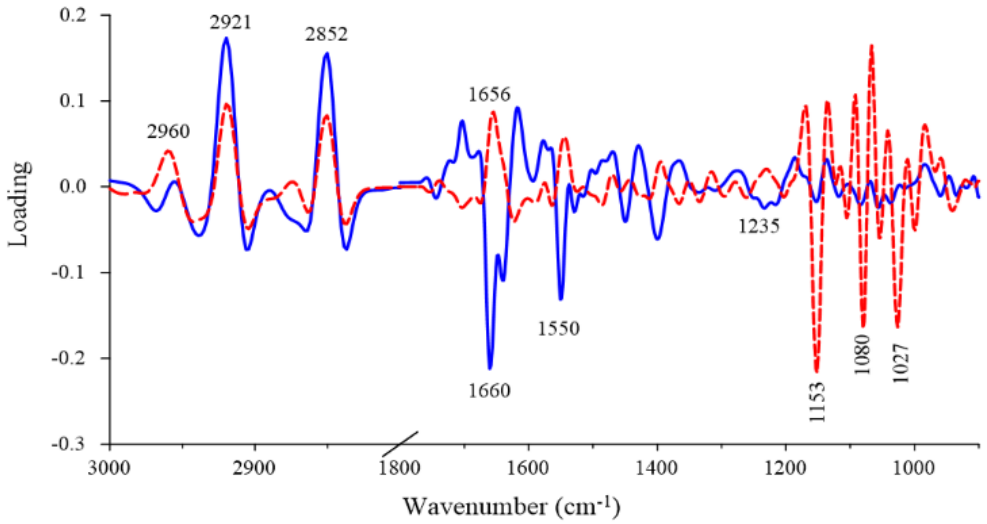

Figure 6 Loading plot of spectrum from treated *B. subtilis* cells.

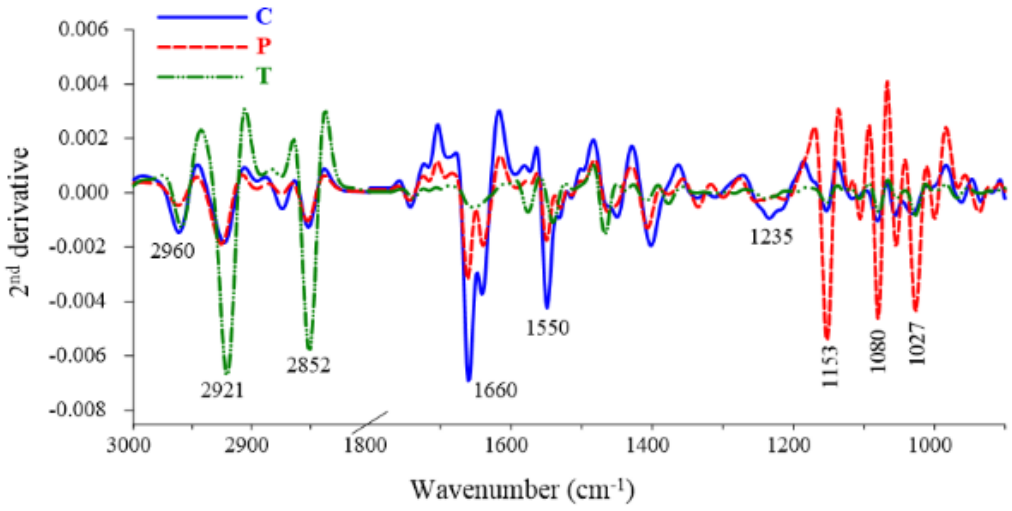

Figure 7 Average spectrum from 2nd derivative of treated *B. subtilis* cells. When sample C is control or untreated cells, sample P is positive control or tetracycline treated cells, and sample T is testing sample or ETE treated cells.

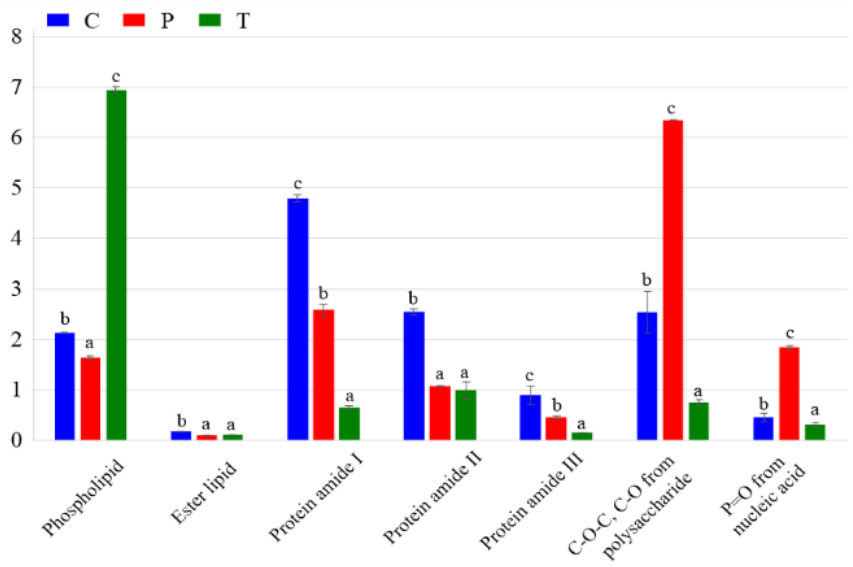

Figure 8 Area under the peaks of functional groups from treated *B. subtilis* cells. When sample C is control or untreated cells, sample P is positive control or tetracycline treated cells, and sample T is testing sample or ETE treated cells. The a, b, and c are significant difference between samples C, P and T when p-value ≤ 0.05.

Table 4 Integral area indicating biomolecules of treated *B. subtilis* cells.

Functional groups	Integral area		
	C	P	T
Phospholipid (3,000 - 2,800 cm^{-1})	2.1378 ± 0.0092^{b}	1.6410 ± 0.0362^{a}	6.9435 ± 0.0630^{c}
Ester lipid (1,740 cm^{-1})	0.1784 ± 0.0049^{b}	0.0989 ± 0.0061^{a}	0.1061 ± 0.0027^{a}
Protein amide I (1,700 - 1,600 cm^{-1})	4.7901 ± 0.0707^{c}	2.5926 ± 0.1192^{b}	0.6421 ± 0.0442^{a}
Protein amide II (1,600 - 1,500 cm^{-1})	2.5467 ± 0.0559^{b}	1.0724 ± 0.0205^{a}	0.9945 ± 0.1751^{a}
Protein amide III (1,300 - 1,200 cm^{-1})	0.8958 ± 0.1852^{c}	0.4620 ± 0.0282^{b}	0.1507 ± 0.0152^{a}
C–O–C, C–O from polysaccharide (1,200-900 cm^{-1})	2.5364 ± 0.4135^{b}	6.3432 ± 0.0089^{c}	0.7516 ± 0.0576^{a}
P = O from nucleic acid (1,080 cm^{-1})	0.4537 ± 0.0852^{b}	1.8442 ± 0.0417^{c}	0.3095 ± 0.0369^{a}

Note: Sample C is control or untreated cells, sample P is positive control or tetracycline treated cells, and sample T is testing sample or ETE treated cells. The a, b, and c are significant difference between samples C, P, and T when p-value < 0.05.

Regarding antibacterial activity, the ETE exhibited stronger effects than the other extracts. SEM and TEM analyses revealed that the ETE induced a similar pattern of cell damage as tetracycline, a bactericidal antibiotic. The ETE caused damage to bacterial biomolecules, including those in the cytoplasm and cell wall. Tetracycline inhibits protein synthesis by preventing the binding of aminoacyl-tRNA to the ribosomal acceptor (A) site, which disrupts the synthesis of proteins, enzymes, DNA, and cell membrane components, leading to bacterial cell damage or lysis. Furthermore, the filamentous appearance of ETE-treated cells observed in SEM may suggest interference with cell division, possibly by targeting DNA or septal cell wall synthesis [26]. This observation was supported by TEM images showing a thinner cell wall and elongated shape, which could indicate abnormal cell division or compromised septum formation. These findings imply that that the ETE may disrupt bacterial cell functions in a manner similar to tetracycline. The filamentous morphology observed in ETE-treated bacteria suggests a possible stress response; however, further studies would be needed to confirm its role as a resistance mechanism.

The FT-IR spectra further corroborated these observations by revealing distinct biochemical changes

in *B. subtilis* cells after treatment. Tetracycline treatment led to increased intensities in nucleic acid and polysaccharide bands, along with decreased signals in protein amide I, II, III, phospholipid, and ester-lipid regions. These changes reflect its known mechanism of action—inhibiting protein and DNA synthesis by binding to the ribosomal A site—which results in reduced protein expression and nucleic acid accumulation. The observed increase in polysaccharide bands may also indicate enhanced exopolysaccharide production, potentially as a protective biofilm barrier to limit antibiotic penetration [27,28]. In contrast, ETE treatment induced broader biochemical alterations. FT-IR peak area analysis showed significant shifts in lipid CH stretching, protein amide, and nucleic acid-associated regions, suggesting that ETE disrupts membrane integrity, denatures proteins, and damages nucleic acids. These findings highlight that ETE exerts antimicrobial effects through mechanisms distinct from those of tetracycline.

In contrast, the ETE treatment resulted in a notable increase in phospholipid spectral bands compared to the control. This finding is consistent with the SEM and TEM results, where ETE-treated cells exhibited a filamentous morphology. The TEM images also showed that the cell wall was thinner than that of untreated cells, which may be due to elongation during filamentation. Some cells appeared to lack visible septa or exhibited incomplete division planes, supporting the hypothesis that ETE disrupted normal cell division. This cell shape alteration likely led to an increase in phospholipid production, as phospholipids are precursors to plasma membrane formation. Changes in cell shape and size are known to be part of a drug resistance mechanism [29]. In the presence of antibiotics, increasing cell volume may dilute the antibiotic concentration within the cell, while a broader cell surface enhances nutrient uptake, promoting cell survival in nutrient-rich environments. In nutrient-poor environments, cells may adapt by transforming their shape to prevent antibiotic influx. Similar transformations to longer or filamentous shapes have been observed in *B. subtilis* following treatment with various antibiotics [30]. This shape change is an adaptive response that enhances survival under chemical or antibiotic stress. The type of antibiotic treatment can also influence the mechanism behind cell shape alterations [26]. Although the ETE demonstrated antibacterial activity, its efficacy was lower than tetracycline based on inhibition zone sizes and the extent of bacterial cell disruption. However, the ETE offers potential advantages such as a complex mixture of bioactive compounds that may reduce the likelihood of resistance development, as well as being a plant-based alternative that could be sustainably sourced. Potential disadvantages include variability in phytochemical content, lower potency compared to conventional antibiotics, and the need for further standardization and safety evaluation before therapeutic application. Long filamentous cells may arise from SOS responses that inhibit cell division due to DNA-targeting antibiotics [31-33]. Cell wall-targeting antibiotics, such as penicillin, prevent peptidoglycan and septal cell wall synthesis, leading to the formation of longer filamentous cells [34].

The FT-IR spectra of ETE-treated cells revealed decreases in protein amide I, II, III, polysaccharide, nucleic acid, and ester-lipid bands compared to the control, suggesting that ETE may inhibit the synthesis of proteins, cell walls, and DNA. The changes in cell shape to a filamentous form likely represent a defense mechanism to dilute the extract's concentration inside the cells and increase nutrient uptake. However, while FT-IR spectra and electron microscopy provided indirect evidence of disruption to bacterial proteins, nucleic acids, and cell wall components, this study did not include direct molecular assays to identify specific targets such as DNA replication enzymes or structural proteins. Further molecular studies, including transcriptomic or proteomic analyses, are needed to confirm these hypotheses and elucidate the precise antibacterial mode of action of the ETE.

Conclusions

The *C. wattii* extract in this study contained flavonoids, phenolics, tannins, and the lycorine alkaloid. These extracts exhibited antibacterial activity, with the ethanolic extract showing the most pronounced effects. Based on these findings, the ethanolic extract was selected for further investigation of its bactericidal activity against *B. subtilis*. The proposed mechanism of action suggests that the ethanolic extract kills bacterial cells by interfering with the synthesis of proteins, cell walls, and DNA. In response, the bacterial cells appear to protect themselves by elongating their shape, which

helps dilute the extract concentration and increase nutrient uptake.

Although lycorine was quantified, its stereoisomeric composition was not determined, and future work will include chiral analyses to identify and quantify specific isomers contributing to the observed activity. Future studies will focus on investigating the molecular mechanisms behind the antibacterial activity of *C. wattii* extract and lycorine to further elucidate their mode of action. Future investigations will include antibiotic-resistant and additional Gram-negative bacterial strains to comprehensively evaluate the antibacterial potential of *C. wattii* extracts. These findings support the potential of *C. wattii* extract as a natural source for antibacterial agent development, encouraging further research on formulation, safety, and therapeutic applications.

Acknowledgements

The authors would like to acknowledge Dr. Chakkrapong Rattamanee for plant identification. This research was funded by Burapha University and Thailand Science Research and Innovation (TSRI) (Grant No. 53/2565).

Declaration of Generative AI in Scientific Writing

The authors used a generative AI tool (ChatGPT, OpenAI) solely for English grammar and language improvement. The scientific content, data interpretation, and conclusions were entirely developed by the authors.

CRediT Author Statement

Sirilak Kamonwannasit: Methodology, Data curation, Formal analysis, Writing- Reviewing and Editing.

Bung-on Prajanban: Formal analysis, Writing- Reviewing and Editing.

Orrasa Prasitnok: Formal analysis, Writing- Reviewing and Editing.

Piaw Phatai: Formal analysis, Writing- Reviewing and Editing.

Agarat Kamcharoen: Conceptualization, Supervision, Writing- Reviewing and Editing, Project administration.

References

[1] N Kumar, M Kumar Mishra and OP Agrawal. *In-vitro* antioxidant activity of hydroalcoholic extract of *Crinum latifolium* using different method. *International Journal of Health Sciences* 2022; **6(S3)**, 9475-9481.

[2] M Salihu, GE Batiha, KI Kasozi, GD Zouganelis, SMZ Sharkawi, EI Ahmed, IM Usman, H Nalugo, JJ Ochieng, I Ssengendo, OS Okeniran, T Pius, KR Kimanje, ES Kegoye, R Kenganzi and F Ssempijja. *Crinum jagus* (J. Thomps. Dandy): Antioxidant and protective properties as a medicinal plant on toluene-induced oxidative stress damages in liver and kidney of rats. *Toxicology Reports* 2022; **9(31)**, 699-712.

[3] LC Silva, AF Correia, JV Gomes, W Romão, LC Motta, CW Fagg, PO Magalhães, D Silveira, YM Fonseca-Bazzo. Lycorine Alkaloid and *Crinum americanum* L. (Amaryllidaceae) extracts display antifungal activity on clinically relevant *Candida* species. *Molecules* 2022; **27(9)**, 2976.

[4] BY Kianfé, J Kühlborn, RT Tchuenguem, BT Tchegnitegni, BK Ponou, J Groß, RB Teponno, JP Dzoyem, T Opatz and LA Tapondjou. Antimicrobial secondary metabolites from the medicinal plant *Crinum glaucum* A. Chev. (Amaryllidaceae). *South African Journal of Botany* 2020; **133(10)**, 161-166.

[5] B Georgiev, B Sidjimova and S Berkov. Phytochemical and cytotoxic aspects of Amaryllidaceae alkaloids in *Galanthus* species: A review. *Plants* 2024; **13(24)**, 3577.

[6] MJM Paiva, GNL Nascimento, IAM Damasceno, TT Santos and D Silveira. Pharmacological and toxicological effects of Amaryllidaceae. *Brazilian Journal of Biology* 2023; **83(2)**, e277092.

[7] J Zhou, IA Stringlis, J Wen, Y Liu, S Xu and R Wang. Interplay between Amaryllidaceae alkaloids, the bacteriome and phytopathogens in *Lycoris radiata. New Phytologist* 2024; **241(5)**, 2258-2274.

[8] N Barghout, N Chebata, S Moumene, S Khennouf, A Harbi and EH Di. Antioxidant and antimicrobial effect of alkaloid bulbs extract of *Polianthes tuberosa* L. (Amaryllidaceae) cultivated in Algeria. *Journal of Drug Delivery and Therapeutics* 2020; **10(4)**, 44-8.

[9] TT Alawode, L Lajide, BJ Owolabi and MT Olaleye. Investigation of bulb extracts of *Crinum jagus* for antibacterial and antifungal activities. *Journal of Applied Sciences and Environmental Management* 2021; **25(1)**, 113-117.

[10] A Di Sotto, M Valipour, A Azari, S Di Giacomo and H Irannejad. Benzoindolizidine alkaloids tylophorine and lycorine and their analogues with antiviral, anti-Inflammatory, and anticancer properties: Promises and challenges. *Biomedicines* 2023; **11(10)**, 2619.

[11] S Kamonwannasit, B Prajanban, A Kamcharoen. Modulatory effect of Plab Plueng Khao (*Crinum wattii*) bulb extract on antioxidant activity and pro-inflammatory mediators. *Huachiew Chalermprakiet Science and Technology Journal* 2023; **9(1)**, 28-43.

[12] N Nasim, IS Sandeep and S Mohanty. Plant-derived natural products for drug discovery: Current approaches and prospects. *The Nucleus* 2022; **65(5)**, 399-411.

[13] N Chaachouay and L Zidane. Plant-derived natural products: A source for drug discovery and development. *Drugs Drug Candidates* 2024; **3(1)**, 184-207.

[14] M Ahmad, M Tahir, Z Hong, MA Zia, H Rafeeq, MS Ahmad, S Rehman and J Sun. Plant and marine-derived natural products: sustainable pathways for future drug discovery and therapeutic development. *Frontiers in Pharmacology* 2025; **15**, 1497668.

[15] K Sawangjaroen and K Keereevong. Spasmolytic effect of papaya (*Carica papaya* L.) leave alkaloid on isolated rat myometrial contraction *in vitro*. *Trends in Sciences* 2022; **19(4)**, 2684.

[16] ZH Pu, D Min, X Liang and C Peng. Total alkaloids from the rhizomes of *Ligusticum striatum*: A review of chemical analysis and pharmacological activities. *Natural Product Research* 2022; **36(13)**, 3489-3506.

[17] GN Pham and H Nguyen-Ngoc. Fissistigma genus – a review on phytochemistry and pharmacological activities. *Natural Product Research* 2021; **35(23)**, 5209-5223.

[18] S Tan, MG Banwell, WC Ye, P Lan and LV White. The inhibition of RNA viruses by amaryllidaceae alkaloids: Opportunities for the development of broad-spectrum anti-coronavirus drugs. *Chemistry: An Asian Journal* 2022; **17(4)**, e202101215.

[19] TE Sebola, NC Uche-Okereafor, L Mekuto, MM Makatini, E Green and V Mavumengwana. Antibacterial and anticancer activity and untargeted secondary metabolite profiling of crude bacterial endophyte extracts from *crinum macowanii* baker leaves. *International Journal of Microbiology* 2020; **2020(1)**, 8839490.

[20] ZU Zango, A Garba, FB Shittu, SS Imam, A Haruna, MU Zango, IA Wadi, U Bello, H Adamu, BE Keshta, DO Bokov, O Baigenzhenov and A Hosseini-Bandegharaei. A state-of-the-art review on green synthesis and modifications of ZnO nanoparticles for organic pollutants decomposition and CO_2 conversion. *Journal of Hazardous Materials Advances* 2025; **17**, 100588.

[21] MA Uddin, X Yuan, L Wang, H Yu, H Wang, X Yuan, BE Keshta, A Basit, C Ouyang, Y Yuan, Y Zheng, J Hu and J Feng. Biomass-derived organonanomaterials as contrast agents for efficient magnetic resonance imaging. *ACS Applied Bio Materials* 2024; **7(12)**, 8479-8488.

[22] S Palaniyappan, A Sridhar, Z Abdul Kari, G Tellez-Isaias and T Ramasamy. Evaluation of phytochemical screening, pigment content, in vitro antioxidant, antibacterial potential and GC-MS metabolite profiling of green seaweed *Caulerpa racemosa*. *Marine drugs* 2023; **21**, 278.

[23] I Ivanov, S Berkov and A Pavlov. Improved HPLC metod for the determination of amaryllidaceae alkaloids. Biotechnol. *Biotechnology & Biotechnological Equipment* 2009; **23(S1)**, 809-813.

[24] W Tafroji, NI Margyaningsih, MM Khoeri, WT Paramaiswari, Y Winarti, K Salsabila, HFM Putri, NC Siregar, A Soebandrio and D Safari. Antibacterial activity of medicinal plants in Indonesia on *Streptococcus pneumoniae*. *PLoS One* 2022; **17(9)**, e0274174.

[25] HM Alkreathy and A Esmat. Lycorine ameliorates thioacetamide-induced hepatic fibrosis in rats: Emphasis on antioxidant, anti-inflammatory, and STAT3 inhibition effects. *Pharmaceuticals* 2022; **15(3)**, 369.

[26] C Cylke, F Si and S Banerjee. Effects of antibiotics on bacterial cell morphology and their physiological origins. *Biochemical Society Transactions* 2022; **50(5)**, 1269-1279.

[27] A Penesyan, IT Paulsen, MR Gillings, S Kjelleberg and MJ Manefield. Secondary effects of antibiotics on microbial biofilms. *Frontiers in Microbiology* 2020; **11**, 2109.

[28] T Stachurová, K Malachová, J Semerád, M Sterniša, Z Rybková and SS Možina. Tetracycline induces the formation of biofilm of bacteria from different phases of wastewater treatment. *Processes* 2020; **8(8)**, 989.

[29] N Ojkic, D Serbanescu and S Banerjee. Antibiotic resistance via bacterial cell shape-shifting. *mBio* 2022; **13(3)**, e00659-22.

[30] N Ojkic and S Banerjee. Bacterial cell shape control by nutrient-dependent synthesis of cell division inhibitors. *Biophysical Journal* 2021; **120(11)**, 2079-2084.

[31] S Ansari, CW James, LB Amy, GD Iain, C Burke and JH Elizabeth. A newly identified prophage gene, *ymfM*, causes SOS-inducible filamentation in *Escherichia coli*. *Journal of Bacteriology* 2021; **203(11)**, e00646-20.

[32] N Ojkic, E Lilja, S Direito, A Dawson, RJ Allen and B Waclaw. A roadblock-and-kill mechanism of action model for the DNA-targeting antibiotic ciprofloxacin. *Antimicrobial Agents and Chemotherapy* 2020; **64(9)**, e02487-19.

[33] Z Yu, ECA Goodall, IR Henderson and J Guo. Plasmids can shift bacterial morphological response against antibiotic stress. *Advanced Science* 2023; **10(2)**, 2203260.

[34] S Banerjee, K Lo, N Ojkic, R Stephens, NF Scherer and AR Dinner. Mechanical feedback promotes bacterial adaptation to antibiotics. *Nature Physics volume* 2021; **17(3)**, 403-409.

Supplementary Material

Table 1S Gradient elution system employed for HPLC analysis of lycorine.

Time (min)	Solvent A (%)	Solvent B (%)	Flow rate (mL/min)
0	90	10	0.4
11	69	31	0.3
15	30	70	0.5
16	10	90	0.5
18	10	90	0.5
19	90	10	0.5
25	90	10	0.5